J Mol Model (2011) 17:1877–1890
DOI 10.1007/s00894-010-0883-5

ORIGINAL PAPER

Computational study of the Na^+/H^+ antiporter from *Vibrio parahaemolyticus*

Assaf Ganoth · Raphael Alhadeff · Isaiah T. Arkin

Received: 13 May 2010 / Accepted: 19 October 2010 / Published online: 24 November 2010

Abstract Sodium proton antiporters are ubiquitous membrane proteins that catalyze the exchange of Na^+ for protons throughout the biological world. The *Escherichia coli* NhaA is the archetypal Na^+/H^+ antiporter and is absolutely essential for survival in high salt concentrations under alkaline conditions. Its crystal structure, accompanied by extensive molecular dynamics simulations, have provided an atomically detailed model of its mechanism. In this study, we utilized a combination of computational methodologies in order to construct a structural model for the Na^+/H^+ antiporter from the gram-negative bacterium *Vibrio parahaemolyticus*. We explored its overall architecture by computational means and validated its stability and robustness. This protein belongs to a novel group of NhaA proteins that transports not only Na^+ and Li^+ as substrate ions, but K^+ as well, and was also found to miss a β-hairpin segment prevalent in other homologs of the *Bacteria* domain. We propose, for the first time, a structure of a prototype model of a β-hairpin-less NhaA that is selective to K^+. Better understanding of the *Vibrio parahaemolyticus* NhaA structure-function may assist in studies on ion transport, pH regulation and designing selective blockers.

Keywords Antiporting · Membrane proteins

Assaf Ganoth and Raphael Alhadeff have an equal contribution to this work.

A. Ganoth · R. Alhadeff · I. T. Arkin (✉)
Department of Biological Chemistry, The Alexander Silberman Institute of Life Sciences, The Hebrew University of Jerusalem, Edmund J. Safra Campus Givat-Ram, Jerusalem 91904, Israel
e-mail: arkin@huji.ac.il

A. Ganoth
e-mail: assaf.ganoth@mail.huji.ac.il

R. Alhadeff
e-mail: raphael.alhadeff@mail.huji.ac.il

Introduction

Living cells are crucially dependent on processes that regulate their intracellular pH, Na^+ content and consequently volume. Sodium proton (Na^+/H^+) antiporting, first discovered in 1974 [1], plays a primary role in maintaining the homeostasis of pH and [Na^+], the latter having a pivotal impact on cell volume, as well. Proteins capable of performing this antiporting function are found ubiquitously in plants, animals and microorganisms, and are present in cell cytoplasmic membranes and in the membranes of many eukaryotic organelles [2]. Moreover, it was suggested, based on the antiporter's involvement in homeostasis of [Na^+] and pH, that a detection mechanism exists, enabling the antiporter to sense its surrounding and adjust to it [3].

Numerous distinct genes that encode Na^+/H^+ antiporters from several bacterial species, such as *Escherichia coli* [4], *Vibrio parahaemolyticus* [5], *Bacillus firmus* [6] and *Enterococcus hirae* [7], have been identified. One such antiporter is the *Escherichia coli* Na^+/H^+ antiporter A, named NhaA [8]. In *Escherichia coli,* NhaA is the only member of the Nha family absolutely required for survival in alkaline conditions in the presence of high external [Na^+] [9].

The protein's crystal structure was solved to 3.45 Å using X-ray crystallography [10]. Only residues 9 through 384 (out of 388 amino acids) can be seen in the electron density, whereas both termini are exposed to the cytoplasm. Twelve trans membrane segments (TMSs) that are connected by extra-membranous loops are found, two of which (IV and XI) are of higher interest. The TMSs IV/XI assembly is composed of two oppositely oriented discontinuous seg-

ments, each in turn composed of a short α-helix, a short unfolded chain, and another short α-helix. Two funnels can be observed; a negatively charged funnel opens from the cytoplasmic face and ends in the middle of the membrane at the putative ion-binding site (D164) and a smaller narrower funnel spans from the periplasm toward the middle of the membrane. The non canonical arrangement of TMSs IV/XI, together with the fact that two funnels from both sides of the protein converge into this assembly, implies that it plays an important role in the protein's activity. At the periplasmic side of the protein, loop I-II, containing a β-hairpin, forms together with the other loops a rigid periplasmic face parallel to the membrane. At its cytoplasmic side, many helices protrude into the cytoplasm forming a rough cytoplasmic face.

Escherichia coli NhaA pH regulation is applied to the antiporter activity, reducing it by more than three orders of magnitude when pH is lowered from 8.5 (maximal activity) to 6.5 [11]. This regulation is a common characteristic of many Na^+/H^+ transporters and requires a detection domain within the protein, a so called "pH sensor", which under different protonation states leads to conformational changes of the protein, affecting its activity [12, 13]. At NhaA, the "pH sensor" appears to be located at the entry of the cytoplasmic funnel, and it was suggested that several residues (such as E78, E252, H253 and H256) constitute a critical component of it [10]. The importance of the electrostatic interactions between the "pH sensor" and the cation binding site were reported by Olkhova et al. [14], assigning different roles to D163 and D164 at the interaction. *Vibrio parahaemolyticus* NhaA shares a similar pH-activity profile [15] and presumably possesses a "pH sensor" as well.

The coupling between the pH sensing and the conformational changes at NhaA was found to be mediated by reorganization of TMS X [16, 17]. Based on a cys-replacement assay, it was revealed that the central conserved residues in TMS X are of high importance to NhaA's antiporting mechanism, and computational analysis identified a distinct pH-induced bend of TMS X.

NhaA physiologically functions as a dimer, yet, the monomer is fully active in isolated membrane vesicles and supports growth of cells under stress conditions of growth [18]. A model of its dimer conformer, based upon intermolecular cross-linking [19], electron spin resonance studies [20] and cryo-electron microscopy of two-dimensional crystals [21], was recently suggested [22]. According to this model, the dimer interface is composed of the two β-hairpins belonging to the two monomers, forming an anti-parallel β-sheet at the periplasmic side of the molecule.

Previous mutation experiments showed that D133, D163 and D164 are essential to NhaA's activity [23]. This finding suggested that these aspartic acid residues, adjacent to the TMSs IV/XI assembly, take part in the transport of ions along the antiporter. Therefore, it was sought to investigate the movement of Na^+ ions out of the vestibules under different protonation states of D163 and D164 and find the functional difference between them. Recent molecular dynamics (MD) simulations on *Escherichia coli* NhaA have suggested a possible mechanism for the ion exchange [24]. According to the proposed mechanism, D164 serves as the Na^+-binding site while D163 serves as the molecular "switch" between the conformations of the protein. Specifically, when D163 is deprotonated it is accessible to the periplasm and D164 is accessible to the cytoplasmic side of the protein. Conversely, when D163 is neutral it is accessible to the cytoplasm, while D164 is accessible to the periplasm. This concerted change facilitates the pumping function of the protein, as well as its electrogenic stoichiometry [24].

Vibrio parahaemolyticus is a slightly halophilic marine bacterium that naturally inhabits coastal waters and can cause illness resulting from eating contaminated shellfish, or, less frequently, through open wound exposure to sea water (*e.g.*, [25]). In the United States, *Vibrio parahaemolyticus* is the most common Vibrio species isolated from humans, as well as the most frequent cause of Vibrio-associated gastroenteritis [26, 27].

Vibrio parahaemolyticus is of special interest not only because of its illness causing potential but also due to its broad antiporter selectivity. In contrast to the *Escherichia coli* NhaA, the *Vibrio parahaemolyticus* NhaA is able to use not only Na^+ or Li^+ as its substrate ion but also K^+ [15]. Also, *Vibrio parahaemolyticus* NhaA belongs to a group of antiporters that are missing a sequence that corresponds to a β-hairpin, compared to the archetype. Since the structure of the NhaA of *Vibrio parahaemolyticus* has yet to be determined, the aim of this current research is to propose a prototype model structure of the protein that may represent this out-group of NhaA proteins. This model might help in further characterizing NhaA's functions and subsequently achieve insights into its pH-regulation, dimerization traits and selectivity basis.

The current study involves a variety of computational techniques used to suggest a model for and characterize the Na^+/H^+ antiporter from *Vibrio parahaemolyticus*. Firstly, we performed a wide spectrum multiple sequence alignment analysis, constructed a phylogenetic tree of the *Bacteria* domain and mapped the *Vibrio parahaemolyticus* NhaA. Based on the results of our phylogenetic study, we applied a homology modeling procedure in order to generate an initial model for the protein's structure. Then, we evaluated the quality of the structure using evolutionary conservation data and performing atomic-level MD simulations as previously suggested by [28, 29], respectively.

We computationally analyzed the MD-derived structure while comparing it to its MD-derived counterpart structure of the *Escherichia coli* NhaA. We calculated the secondary structure, computed the main eigenvectors of movement, measured the vestibule size, determined the accessibly of the ion binding site and mapped the electrostatic potential. This series of analyses, which underlines principle features of the NhaA from *Vibrio parahaemolyticus*, highlights its similarity, albeit with a few differences, to the NhaA from *Escherichia coli*. We propose that the model for the *Vibrio parahaemolyticus* NhaA presented at this study can be considered as a working tool to aid theoretical and experimental studies.

Methods

Multiple sequence alignment and phylogenetic tree construction

Multiple sequences were retrieved and aligned using the Pfam database [30]. All sequences from the *Bacteria* domain were downloaded, sorted [31], and further analyzed using an in-house purpose written perl script. In short, for each of these sequences the script counts the number of amino acids between the end of TMS I and the beginning of TMS II. Only sequences longer than 300 residues overall were selected (roughly the minimum for all the helices and connecting loops), from which only these with TMSs I-II connecting segment shorter by at least eight residues (compared to the same segment in *Escherichia coli* NhaA) were assigned as missing the β-sheet hairpin. The phylogenetic tree was constructed based on 16S rRNA using version 2.72 of the Mesquite software for evolutionary biology [32].

Homology modeling

The template used to model NhaA from *Vibrio parahaemolyticus* (Entrez accession code ZP 01991281.1) was NhaA from *Escherichia coli* (PDB entry 1ZCD, chain A). The amino acid sequences of the NhaA from both bacteria were aligned using BLAST [33, 34] with the blastp algorithm. Homology models were generated with Modeller 9.4 [35] so that they match the alignment. The model with the best score was assessed for its quality with respect to its energy and stereochemical geometry using Procheck 3.5.4 [36, 37], ProSA-Web [38, 39] and Verify3D [40].

Evolutionary conservation

The conservation score of each residue of the protein was retrieved from the sequence alignment done using Pfam database as presented above, based on Blosum62 scores [41]. The scores were applied on a linear scale and colored from red (score 0) to blue (highest score achieved), through green (half maximal score) using an in-house purpose script.

Simulation system set up

Two simulation systems were prepared, one for the *Vibrio parahaemolyticus* NhaA and the other for the *Escherichia coli* NhaA. The structure of the former was taken after the homology modeling procedure, and that of the latter was downloaded from the PDB (entry 1ZCD [10]). Both proteins were separately embedded in a pre-equilibrated 1-palmitoyl-2-oleoyl-sn-glycero-3-phosphoethanolamine (POPE) bilayer [42], which initially contained 340 lipids and 6729 molecules of SPC water [43], trimmed to 244 lipids and 4237 water molecules and further equilibrated for 2 ns. The antiporter rough axis was aligned perpendicular to the membrane surface and all colliding lipids and water molecules, within 2 Å of the protein, were manually removed (down to 148 lipids and 4035 water molecules for the *Vibrio parahaemolyticus* and 153 lipids and 4032 water molecules for the *Escherichia coli*). The systems' total charge was neutralized by adding K^+ and Cl^- ions to a final concentration of 0.1 M, replacing randomly selected water molecules. Both systems were subjected to rigorous energy minimization using the steepest descent algorithm and a tolerance of 1000 $kJ \cdot mol^{-1} \cdot nm^{-1}$, followed by a minimization using the conjugated gradient algorithm with a sequential decreasing convergence from 100 to 10 $kJ \cdot mol^{-1} \cdot nm^{-1}$. Then, an equilibration stage under positional restraints using a harmonic force constant was conducted. The equilibration procedure began with a force constant of $k = 1000\ kJ \cdot mol^{-1} \cdot nm^{-2}$ for 100 ps, then a force constant of $k = 500\ kJ \cdot mol^{-1} \cdot nm^{-2}$ for 100 ps, and another 100 ps with an unrestrained MD run. After the positional restraint equilibration, the systems were submitted for unbiased MD runs.

MD details

The simulations were conducted using version 3.3.1 of the GROMACS package [44, 45], employing an extended version of the GROMOS53a6 force field [46]. All simulations were conducted using the LINCS algorithm [47] to constrain bond lengths and angles of hydrogen atoms, allowing a time step of 2 fs. Simulations were run using Berendsen temperature coupling at 310 K employing a coupling constant of $\tau = 0.1$ ps. Pressure was kept constant by applying semi-isotropic coupling at 1 bar with a coupling constant of $\tau = 1$ ps, differentiating the z-axis (the membrane normal). A cutoff of 1.2 nm was used for van

der Waals interactions, while long range electrostatic interactions were computed using the PME algorithm [48].

Essential dynamics

The conformational space spanned by a macromolecule during its equilibrium dynamics can be evaluated by performing a principal component analysis, a.k.a. essential dynamics, on its atomic coordinates [49]. Thus, for the essential dynamics analysis, we considered the first 7 ns of each simulation as an equilibration period, and the remaining 13 ns were used for the analysis. A correlation matrix was constructed based on the coordinates fluctuations of the main-chain atoms. Then, the matrix was diagonalized to obtain the eigenvectors and eigenvalues in order to yield information about the correlated motions of the protein.

Funnel characteristics

Funnel volume of the proteins was evaluated using version 3.1.1 of the program VOIDOO [50, 51] with a probe radius of 1.4 Å. The dihedral angle of the putative Na^+ binding site was measured by the side chain of D164 (C-Cα-Cβ-Cγ).

Electrostatic potential

The electrostatic potential around the protein was calculated for a representative structure from each simulation. We solved the nonlinear Poisson-Boltzmann (PB) equation through the use of the adaptive Poisson-Boltzmann solver (APBS) software package [52] with a grid spacing of 0.4 Å. Following Olkhova et al. [53], we used dielectric constants of ϵ=4 and ϵ=78.4 for the protein and for the bulk, respectively. For visualization convenience, the NhaA proteins from both bacteria were aligned according to their RMSD prior to the calculation for comparison.

Visualization and analysis

The simulations were visualized with the Visual Molecular Dynamics (VMD) program [54]. The analyses were conducted using in-house VMD Tcl scripts, perl scripts and the GROMACS analyses package tools.

Results and discussion

Multiple sequence alignment and phylogenetic tree

Preliminary sequence alignment revealed that *Vibrio parahaemolyticus* NhaA is shorter than its *Escherichia coli* counterpart in the segment between TMSs I and II by nine amino acids (Fig. 1). To test whether this phenomenon is unique to the *Vibrio parahaemolyticus* antiporter, we performed multiple sequence alignment using NhaA homologs from all the *Bacteria* domain. 681 sequences from the Pfam database were subjected to our analysis (see Methods) and showed that as many as 20% of them lack nine or more amino acids in the inspected segment. Interestingly, the residues in this segment are those that form the β-hairpin loop that is found at the periplasmic face of the protein. Thus, a careful analysis of the obtainable data suggests that this deletion results in a lack of the β-hairpin loop (this issue is elaborated at the homology modeling section below). Indeed, previous work on *Escherichia coli* NhaA had shown that the β-hairpin region is not necessary for protein expression nor activity, and that the protein is active even with its β-sheets removed [55]. Furthermore, nearly all (85%) sequences from the various bacteria, which allegedly lack the β-hairpin, are missing exactly nine amino acids. This implies that the deletion is not random, and that the β-hairpin deleted NhaA group we found here is apparently evolutionarily stable.

We further tested this hypothesis and built a phylogenetic tree based on 16S rRNA and highlighted all the β-hairpin lacking bacteria (Fig. 2). Apparently, there is no phylum with a large majority of deleted β-hairpin proteins (except for *Gemmatimonadetes* which contains only one sequence). However, we see that the β-hairpin missing proteins can be found throughout the *Bacteria* domain (*e.g.*, *Firmicutes* and *Actinobacteria*). A closer look at the *Proteobacteria* phylum reveals that two particular orders (*Rhizobiales* and *Vibrionales*), albeit from different classes, have a large majority of β-hairpin missing proteins within them (as does the single sequence from *Rhodocyclales*). On the other hand, many of the other orders still have at least one representative protein that has its β-hairpin absent (*e.g.*, *Pseudomonadales*). This may hint that the missing β-hairpin trait has been adopted by various bacteria via horizontal gene transfer. To support this theory, we compared similarity and sequence identity between bacteria within the same class, bearing a β-hairpin, with bacteria from a different phylum ("out-group") with their β-hairpin missing. If horizontal gene transfer had happened, we would expect to see a higher similarity to the more distant bacteria based on the common trait of missing a β-hairpin. Indeed, *Vibrio cholerae* from the *Vibrionales* order shows 40% identity and 56% similarity with respect to *Congregibacter litoralis* from the *Congregibacter*, while showing 48% and 65% identity and similarity, respectively, to *Gemmatimonas aurantiaca* from the *Gemmatimonadetes* phylum. Likewise, *Brucella suis* from the *Rhizobiales* order holds 35% and 56% identity and similarity, respectively, with *Rickettsia massiliae* from the

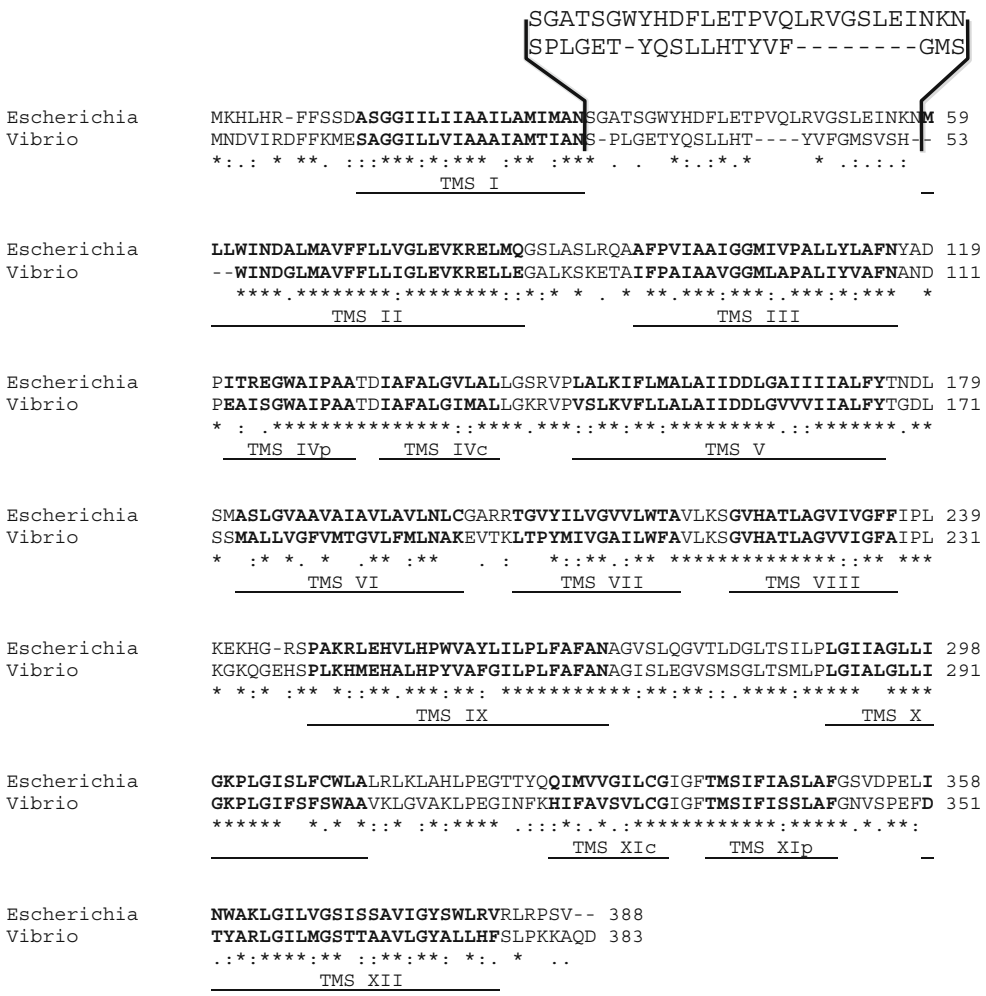

Fig. 1 BLAST sequence alignment between *Escherichia coli* NhaA (PDB entry 1ZCD) and *Vibrio parahaemolyticus* NhaA (Entrez accession code ZP_01991281.1). Stars, colons and dots refer to identical residues, conserved and semi conserved substitutions, respectively. TMSs are sequentially indicated. Inset: Adjustment at the β-hairpin region prior to the construction of the model

Rickettsiales order, compared to 47% and 65% with *Veillonella dispar* from the *Firmicutes* phylum.

To our knowledge, no functional characteristic of lacking β-hairpin has been documented, but the apparent gene transfer may suggest positive selection for it in particular bacteria species. While we cannot deduce the origin of this trait from this finding *per se*, *Vibrionales* seems to be the most probable order from which this trait origins. Further analysis of the topic is beyond the scope of our current research.

Homology modeling

Homology modeling of membrane proteins is similar in nature to that of water soluble proteins [56]. Given that the NhaA of *Vibrio parahaemolyticus* shares a high sequence identity (59%) and similarity (74%) with the NhaA of *Escherichia coli* (Fig. 1; E value=$7{\cdot}10^{-122}$), the NhaA of *Escherichia coli* was selected as a template for the homology modeling process. The extensive sequence resemblance between the proteins ensures a high success of the modeling process.

Since the sequence of the *Vibrio parahaemolyticus* NhaA lacks nine residues between the putative TMSs I and II and in line with the multiple sequence alignment and phylogenetic analyses, we constructed the model of the *Vibrio parahaemolyticus* NhaA without the β-hairpin patch that is present at the *Escherichia coli* NhaA structure. Expectedly, the resulted homology model of *Vibrio parahaemolyticus* NhaA is similar to the template except between TMSs I and II, as noted above. Considering the striking homology at the flanking TMSs (identity 67% and similarity 89%), the difference probably manifests in a lack of the β-hairpin segment in between them at the *Vibrio parahaemolyticus* NhaA.

Model quality assessment

Prior to the MD simulations, the *Vibrio parahaemolyticus* NhaA model structure was evaluated for its quality. The overall G-factor of Procheck was -0.13 and the Ramachandran plot showed that 98.2% of the residues lie in allowed regions (from which 89.0% in the most favored regions). No major stereochemical clashes and bad contacts for main-chain or

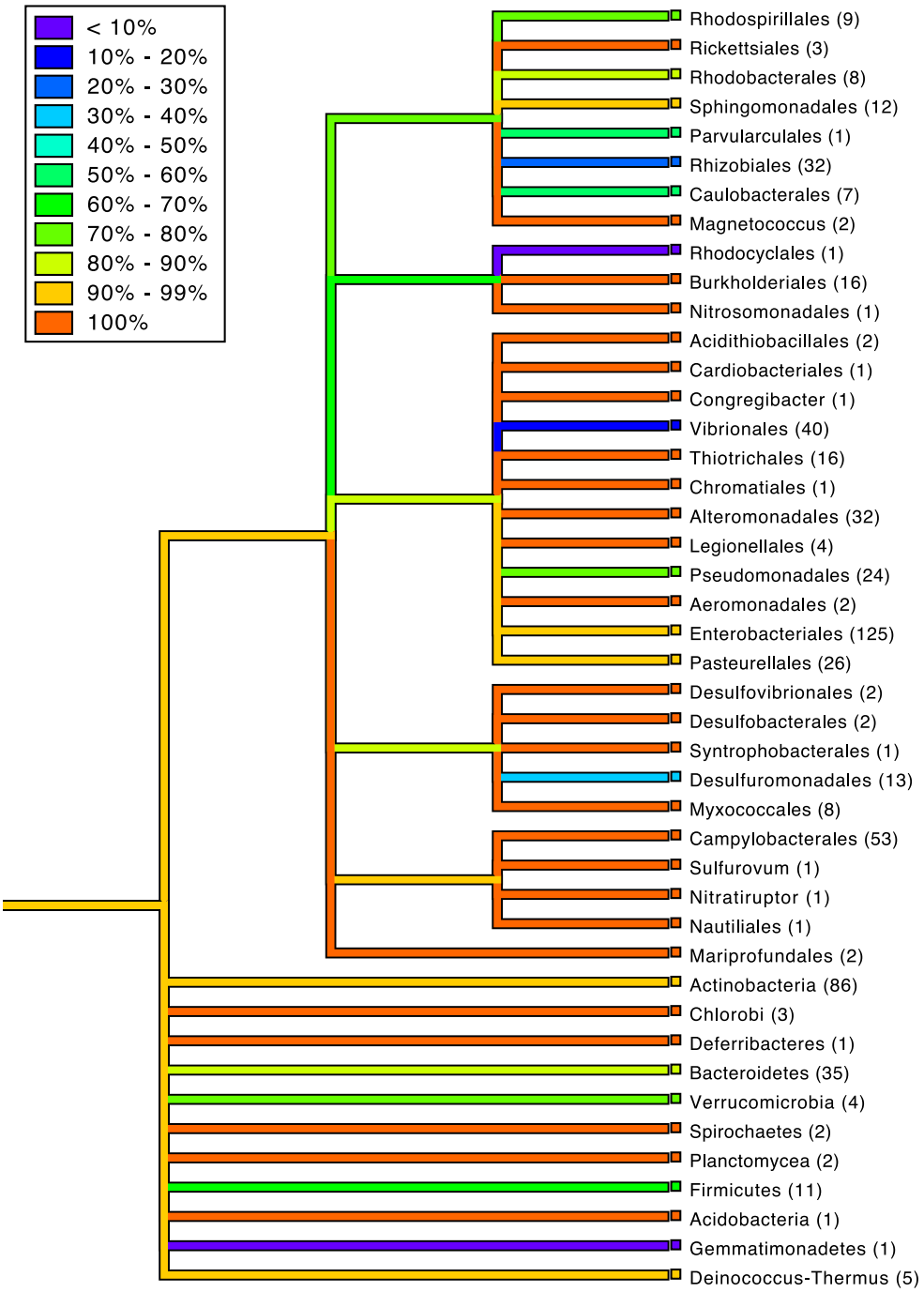

Fig. 2 Phylogenetic tree of selected bacteria based on 16S-rRNA. Depicted in color is the percentage of the genus possessing β-hairpin containing NhaA, and in parentheses is the total number of sequences on which the analysis was done, in each group (Phylum or order). Branch lengths are not to scale

side-chain parameters were detected. Global analysis of the model with ProSA showed a Z-Score of -6.47, implying no significant deviation from the template *Escherichia coli* NhaA structure. The Verify3D analysis indicated a reasonably good sequence-to-structure agreement with an average score of 0.308. Thus, the resulted model of the homology modeling procedure (and before the MD simulations) was a relatively reliable structure.

Evolutionary conservation

In both soluble and membrane proteins, evolutionary conserved residues are typically buried at the protein's core, whereas variable residues are located at its periphery [57]. At membrane proteins, these variable residues are usually found at the TMSs connecting loops or on the protein's surface where they face the membrane lipids or the

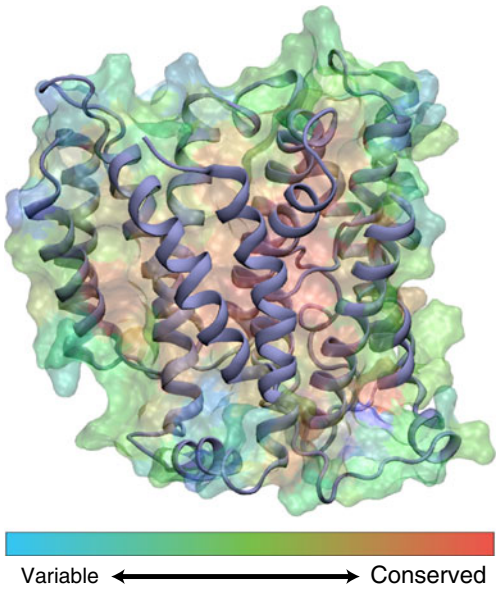

Fig. 3 The evolutionary conservation profile of the Vp-NhaA is mapped on its model structure. The residues are colored by their conservation grade using Blosum62 score. The protein is depicted in navy; an internal slice of the protein is painted according to the scale at the bottom

bulk. Accordingly, evolutionary conservation analyses have been employed to predict structures of membrane proteins and as tool to validate model structures [58, 59]. On the basis of a 744 sequences alignment, we mapped the conservation score of the *Vibrio parahaemolyticus* NhaA (Fig. 3). In line with our expectation, we have found that the most highly-conserved residues are located at the protein's interior where they are lipid-inaccessible, while the most variable residues are found at its periphery. Interestingly, and in accordance with the study of Olkhova et al. [17], residues at the center of TMS X, which are functionally important for the protein's pH-dependent conformational change, are highly-conserved. Not surprisingly, the loops connecting to the β-sheet in the *Escherichia coli* NhaA located at the periphery, are among the least conserved ones. Also, the putative binding site, as well as other key residues mentioned below (see section below) are highly-conserved. Our results highlight that the model we present answers the evolutionary conservation criteria.

Overall three-dimensional structure

MD simulations can be used as a tool to test and examine the quality of homology modeled membrane proteins in cases in which there is low sequence identity and similarity between the template structure and the target [29, 60]. A fortiori, this applies in our study, with 74% sequence similarity. In order to test the resultant model from the homology modeling procedure, we performed a 20 ns MD simulation of the protein embedded in a hydrated membrane and at the presence of physiological salt concentration. Additionally, an MD simulation of 20 ns was performed for the *Escherichia coli* NhaA protein under the same conditions. Representative structures from the 20 ns MD simulation of the *Vibrio parahaemolyticus* NhaA (navy), superimposed with the X-ray structure of the *Escherichia coli* NhaA (yellow), are presented on Fig. 4.

The two structures of the protein from both bacteria closely resemble each other, and the *Vibrio parahaemolyticus* NhaA displays all the distinguishing characteristics of the *Escherichia coli* protein, except for the aforementioned missing β-hairpin region (highlighted in black). The *Vibrio parahaemolyticus* NhaA comprises of twelve TMSs; TMSs IV (orange) and XI (purple) form the unique assembly exactly as at the *Escherichia coli* protein, the N- and C-termini are exposed to the cytoplasm (see below), a funnel opens into the cytoplasm and continues to the middle of the membrane, a shallower funnel opens to the periplasm and is separated from the cytoplasmic funnel by non-polar residues that act as a barrier, the periplasmic face of the protein is flat owing to structured loops and the cytoplasmic face is rough with flexible loops and a few helices that protrude into the cytoplasm. The longer termini apparent in the *Vibrio parahaemolyticus* NhaA do not appear in the crystal structure but exist in the *Escherichia coli* protein itself, roughly of the same length.

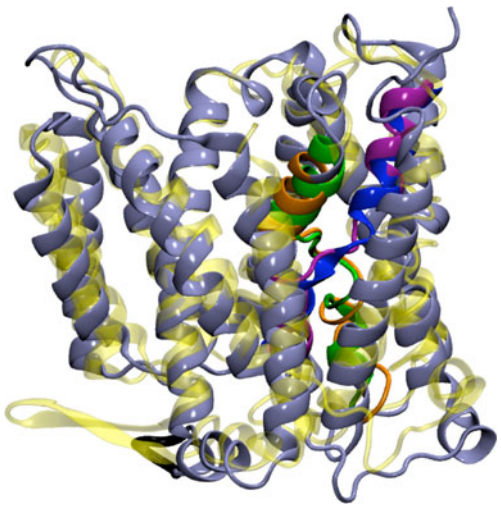

Fig. 4 Schematic diagrams of a representative structure derived from the 20 ns simulation of the *Vibrio parahaemolyticus* NhaA (navy) superimposed to the X-ray structure (PDB entry 1ZCD) of the *Escherichia coli* NhaA (yellow). TMSs IV and XI of the *Vibrio parahaemolyticus* NhaA are colored with orange and purple and these of the *Escherichia coli* with green and blue, respectively. Highlighted in black is the location on the *Vibrio parahaemolyticus* where the β-hairpin of *Escherichia coli* is present

The profound structural difference between the protein of both bacteria is manifested in the β-hairpin, which is present in the *Escherichia coli* but absent in the *Vibrio parahaemolyticus*. It was suggested that its role is to participate in the dimerization process of *Escherichia coli* NhaA [22], and hence the dimerization of the *Vibrio parahaemolyticus* remains an unsolved question. If this protein functions as a dimer, then the interface should be reevaluated and cannot be mediated by the β-hairpin segment alone. Since the dimerization becomes crucial at the *Escherichia coli* only under extreme stress conditions, it may not be a prerequisite for the bacterium's survival at physiological environment.

Regulation of the antiport activity of *Escherichia coli* NhaA requires a "pH sensor", which was found to include residues such as E78, E252, H253 and H256 [14]. These residues are located at the N-terminal side of the cytoplasmic funnel not only at the *Escherichia coli* template but also at the suggested model for the *Vibrio parahaemolyticus* NhaA. Taking into account the high sequence and structure resemblance, it is tempting to suggest that the mechanism for pH regulation of *Vibrio parahaemolyticus* would be the same as previously proposed for *Escherichia coli*. This was experimentally studied by Radchenko et al. [15] who reported the discovery of the *Vibrio parahaemolyticus* NhaA and studied its ion specificity and pH activation profile. A few key other functional residues of the *Escherichia coli* located at TMS II (D65), TMS IV (D133), TMS V (D163, D164) and TMS X (L296, G299, K300, G303) were found to play distinct significant physiological roles [10, 16, 61]. These residues fit to exactly the same helices at the *Vibrio parahaemolyticus* NhaA model structure as well; furthermore, they maintain their orientation throughout the simulations of both proteins. Overall, the architecture of our suggested model for the *Vibrio parahaemolyticus* NhaA retains the distinctive *Escherichia coli* NhaA characteristics.

Stability

We undertook several measures in order to gauge the stability of the proteins' structure as a function of the simulation time. First, deviation of the simulated structure from the initial configuration. Then, fluctuations of each of the proteins' residues, and finally a helix retention analysis. The reference structure for the *Escherichia coli* NhaA was its crystal structure whereas the one for the *Vibrio parahaemolyticus* NhaA was the model obtained from the homology modeling process. Monitoring the time evolution of both systems (Fig. 5a) reveals that the two proteins are stable during the course of the simulation. Qualitatively, the backbone atom RMSD patterns for the

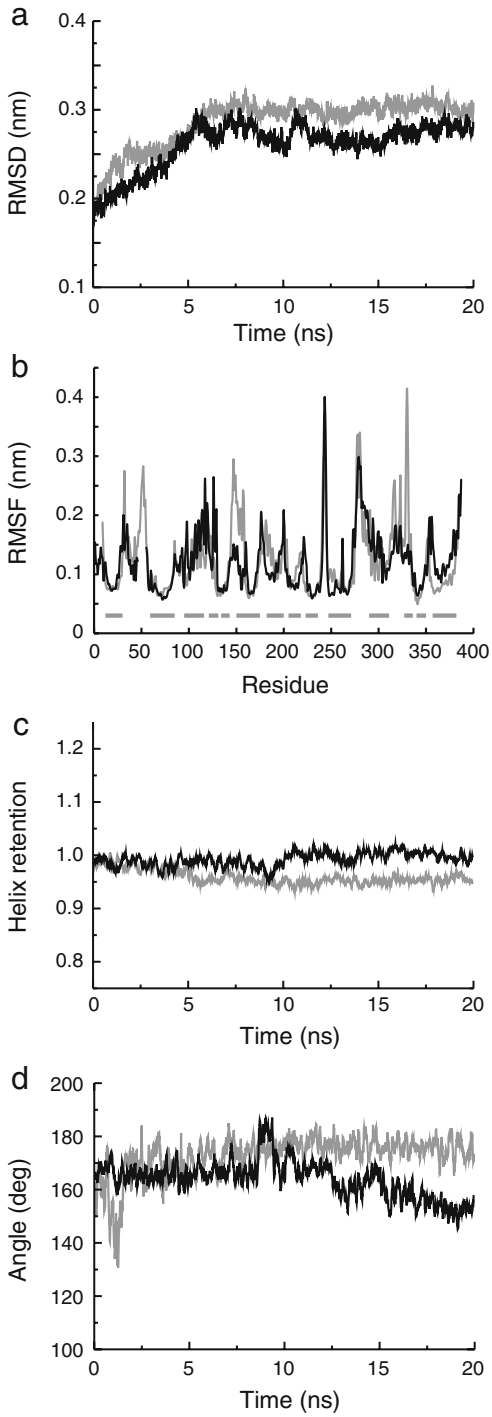

Fig. 5 Analysis of structural parameters of the *Vibrio parahaemolyticus* (black) and *Escherichia coli* (gray) NhaA protein as a function of the 20 ns MD simulation: (a) RMSD for the backbone atoms; (b) RMSF, aligned by sequence, TMSs marked with horizontal bars; (c) Relative helix retention and (d) Accessibility of D164 to the funnel's core

Vibrio parahaemolyticus and for the *Escherichia coli* look similar. They rise over ~6 ns up to a value of ~0.3 nm and stabilize around this value until the end of the simulations. Hence, both RMSD curves imply that the two structures

do not deviate substantially during the simulations and are relatively stable. This was further verified by following the root mean square fluctuation (RMSF) of the proteins (Fig. 5b). Not surprisingly, both curves present relatively mild oscillations. Notably, the structural sections of the proteins, namely their twelve TMSs, are more rigid and confined and tend to be less flexible than other sections (*e.g.*, residues 59-85 of TMS II at both bacteria). Correspondingly, the proteins' unstructured sections show an increased mobility. Thus, at both simulations, the RMSF data indicate larger fluctuations of segments belonging to loops that connect the helices (*e.g.*, residues 237-246 that connect TMS VIII to TMS IX and residues 273-290 that connect TMS IX to TMS X), as well as of residues located at the edges of the α-helical sections (e.g., residue 356 of the *Vibrio parahaemolyticus* NhaA) or edges of the protein (*e.g.*, residue 384 of the *Escherichia coli* NhaA). The dynamics of TMS X during the simulations is not typical for helical segments, and hence it has a relatively high RMSF. At our simulations, it bends and tilts (at a lower and higher extents for the *Escherichia coli* and the *Vibrio parahaemolyticus*, respectively) similarly to the findings of [17].

Next, we followed the helix retention (Fig. 5c) of the proteins as a function of time. A normalized helix retention analysis revealed that both proteins retain their α-helical content throughout the simulation time. The normalized helix retention rate is pretty high, 0.99±0.01 and 0.96±0.01 for the *Vibrio parahaemolyticus* and the *Escherichia coli* NhaA, respectively. This implies that the proteins' secondary structure elements are steady as a function of time, meaning that the vast majority of the TMSs do not unwind.

Essential dynamics

Having demonstrated that the proteins do not exhibit any striking conformational change that is readily observable, we decided to employ analysis of essential dynamics in order to examine what underlying concerted motions we might uncover. Since the introduction of essential dynamics by Berendsen and co-workers in 1993 [49], it has been widely used as a useful technique to explore motions of proteins. Hence, we applied essential dynamics analysis to monitor the principle components of NhaA's motion throughout the simulations (Fig. 6). A close examination of the movements associated with the first and second eigenvectors of the protein, at both proteins, reveals that the helices, which constitute the TMSs, jiggle and tumble along the simulations. No major conformational changes are observed and only minor wiggling and helical fluctuations are detected. However, each eigenvector of each bacterium is characterized by its unique pattern of motions (or absence of them). At the first eigenvector of the *Vibrio parahaemolyticus* NhaA, all TMSs slightly fluctuate except TMSs VII and VIII. Similarly, at the second eigenvector of the *Vibrio parahaemolyticus* NhaA, all TMSs rotate as well except TMSs VI and VIII. Notably, the TMSs that exhibit the highest degree of motion were TMSs III, X and XII at both eigenvectors. The local movements of the *Vibrio parahaemolyticus* NhaA are generally more profound and their extent is more substantial than these of the *Escherichia coli* NhaA. At the first eigenvector of the *Escherichia coli* NhaA, TMSs I, VI and VIII barely move whereas TMSs V, X and XI are characterized by more intense movements. In the

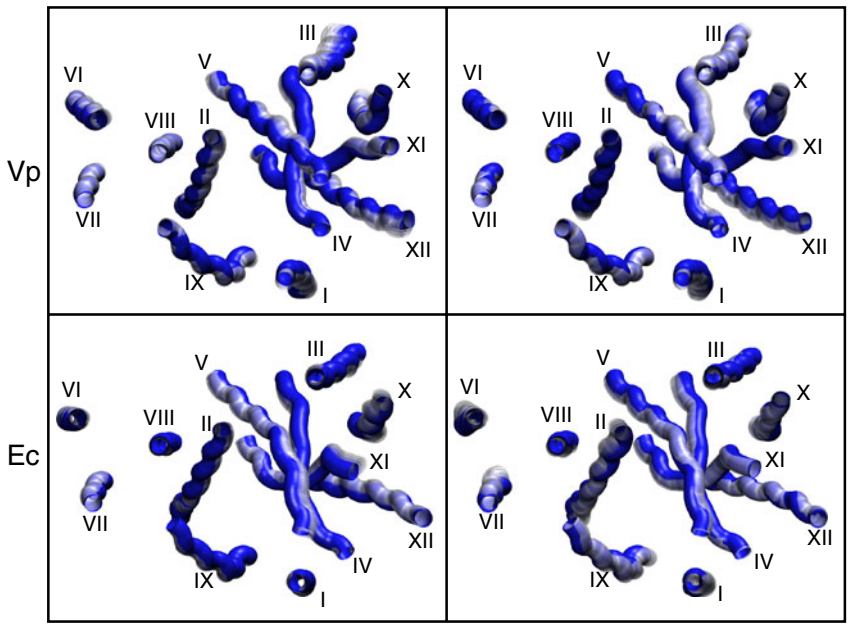

Fig. 6 Visual representation of the results of filtering the simulations trajectories along the principal eigenvectors of the *Vibrio parahaemolyticus* NhaA (top) and the *Escherichia coli* NhaA (bottom). Movements along the first and the second eigenvectors are presented at the left and the right sides of the panel, respectively. The TMSs, which are shown from top view membrane from the periplasm and sequentially numbered with roman numerals, are colored blue and white along their motions

second eigenvector of the *Escherichia coli* NhaA, TMSs III and VIII hardly move whereas TMSs II, VI, VII, IX and X exhibit more considerable movements.

TMSs VI-VIII are of special interest since the β-hairpin, which is absent at the *Vibrio parahaemolyticus* NhaA and present at the *Escherichia coli* NhaA, is structurally found beneath them when one looks from a periplasmic top view. TMS VI rotates only at the first eigenvector of the *Vibrio parahaemolyticus* and at the second eigenvector of the *Escherichia coli*, while at the second eigenvector of the *Vibrio parahaemolyticus* and at the first eigenvector of the *Escherichia coli* is relatively idle. TMS VII is characterized by more intensive motions at both eigenvectors at the *Escherichia coli* rather than at the *Vibrio parahaemolyticus*. Two other TMSs, TMSs VIII and X, present a consistent, yet opposite, pattern of behavior at both eigenvectors of both bacteria NhaA's: TMS VIII is relatively still due to conformational and steric restraints that stabilize it (tight proximity to TMSs II, VI and VII) and because of its internal location at the protein's topology. TMS X is the most motile TMS probably because of its peripheral location at the protein and due to the fact that it flanks long loops (19 and 18 residues at its N- and C- termini, respectively) which makes it less confined to structural constraints. The high motility of TMS X detected by our simulations at a physiological pH, was previously recorded by Olkhova et al. [17] who concluded that TMS X is highly-mobile at MD simulation performed at pH 8.

The main differences between the NhaA structures of both bacteria is seen when one examines the location of TMSs V and VI from the top view membrane (Fig. 6). Regarding TMS V, one should take into account that this is the helix on which D163 (the molecular "switch" between the conformations of the protein) and D164 (the Na^+-binding site) reside [24]. At the *Escherichia coli* protein the C-terminal twists and it loses its linearity, while in the *Vibrio parahaemolyticus* antiporter it is relatively linear. As for TMS VI, in the *Vibrio parahaemolyticus* protein it deviates from the membrane plane; whereas in the *Escherichia coli* antiporter, it is almost perpendicular to the membrane axis. This difference at the tilt of TMS VI is caused by the β-hairpin feature; its absence at the *Vibrio parahaemolyticus* enables TMS VI to change its angle relative to the membrane when compared to the *Escherichia coli* in which it is tightly packed along the membrane axis and cannot tilt due to steric hindrances.

Funnel characteristics

The functionality of both proteins is enabled due in part to a vestibule that opens from the TMSs IV/XI assembly to the cytoplasm and the periplasm. The passage of Na^+ and H^+ is thought to be mediated through the vestibule [10], and hence it serves as the proteins' functional core. One may assume that the selectivity basis of both proteins stems from different funnel sizes, and consequently we followed the volume of the vestibule that spans from the cytoplasm toward the TMSs IV/XI assembly of the proteins. We have found that the funnel size of representative MD-derived structures of the *Vibrio parahaemolyticus* and the *Escherichia coli* NhaAs' are $15.9 \cdot 10^{-3}$ nm^3 and $66.2 \cdot 10^{-3}$ nm^3, respectively. The larger funnel size of the *Escherichia coli* is of high significance in the light of the fact that the NhaA from *Escherichia coli* is permissive only to Na^+ and Li+ whereas that from *Vibrio parahaemolyticus* is more promiscuous and transports K^+ as well. Hence, the specificity mechanism and selectivity basis may not be the vestibule size *per se* and further comprehensive studies and analyses might reveal insights on the subject.

The mode of ion binding is most probably a direct attachment to the carboxyl group of D164 side chain, presumably at its center [24]. Thus, we examined the accessibility of D164 to the vestibule's pore (Fig. 5d). We checked the dihedral angle of its rotamer in order to observe the availability of the ion binding site to the vestibule's space. The dihedral angle of the rotamer of both proteins is stable; 163.9°±6.9 and 172.8°±7.5 for the *Vibrio parahaemolyticus* and the *Escherichia coli* , respectively. These similar values indicate that the side chain of both proteins points toward the funnel space, and hence is capable of functioning as an ion binder.

Electrostatic potential

The NhaA sequences from *Vibrio parahaemolyticus* and the *Escherichia coli* share high identity and similarity, nevertheless there are numerous structural and functional differences between them. To account for the electrostatic similarities and differences, we calculated the electrostatic field surrounding the proteins for a representative structure from each simulation using APBS, where the solutes are treated in atomic detail and the bulk is represented by a continuum model (Fig. 7). The positive (blue) and negative (red) domains for the Coulomb cage are drawn where the electrostatic potential equals 1 kBT/e^- whereas the proteins are shown in gray by vdW representation. Each protein presents distinct positive and negative lobes; the former faces the cytoplasm while the latter faces the periplasm. This is in accord with the positive-inside rule [62] and probably facilitates the right orientation of the protein as it integrates into the membrane. The volume of the positive Coulomb cage around the *Vibrio parahaemolyticus* NhaA is 60.3 nm^3, while the volume of its negative Coulomb cage is 130.3 nm^3. The volume of the positive Coulomb cage around the *Escherichia coli* NhaA is 237.9 nm^3, while the volume of its negative Coulomb cage is 67.3 nm^3.

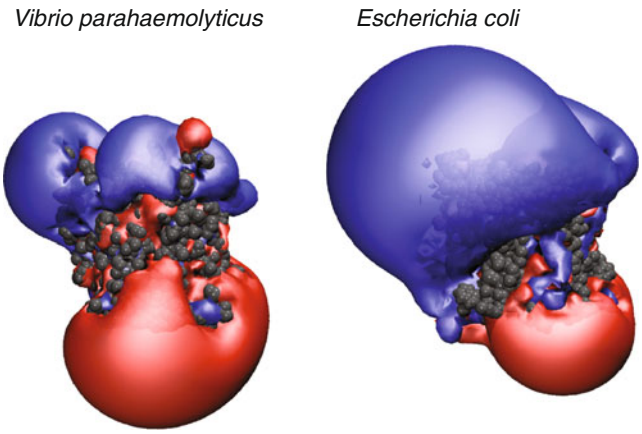

Fig. 7 The electrostatic potential surface of the *Vibrio parahaemolyticus* NhaA (left) and *Escherichia coli* NhaA (right). The Coulomb cages for the positive (transparent blue) and negative (transparent red) domains are drawn at the distance where the electrostatic potential equals ±1 kBT/e^{-}

Apparently, the differences between the electrostatic fields surrounding the proteins are caused by variations in their net charge and charge distribution. The total charge of the *Vibrio parahaemolyticus* NhaA is Z=-1, while that of the *Escherichia coli* NhaA is Z = +3. These differences mainly account for the different volumes of the positive and the negative Coulomb cages. In addition, the proteins differ not only in their total net charge, but in the distribution of the charged residues along them as well. The positively-charged residues at the *Vibrio parahaemolyticus* NhaA are scattered, while these of the *Escherichia coli* NhaA are much more clustered (data not shown) and hence their contribution to its high-volume positive Coulomb cage bulb is profound. This phenomenon is opposite at the *Vibrio parahaemolyticus* protein where its negatively-charged residues are less scattered and tend to cluster at its periplasmic side. The differences between the electrostatic fields of the two proteins may suggest that electrostatic forces can play a role in their functional activities.

The calculation of the electrostatic potential was done by applying an implicit continuum water molecules model with a dielectric constant of ϵ=78.4, yet the NhaA protein is fully embedded in a membrane. How can one reconcile this alleged contradiction? Olkhova et al. [53] explored the effect of pH values on the protonation states of almost 70 titratable residues in NhaA by performing a multi-conformation continuum electrostatic (MCCE) analysis. According to their study, the calculated pKa values for the titratable sites of NhaA were very similar (close to 2%) when their calculations included an implicit modeling of solvent *per-se*, an implicit modeling of solvent embedded into a membrane, an explicit model of solvent or an explicit water molecules with a membrane model. The differences of the four systems they investigated were insignificant, and following their study, we suggest that introduction of a membrane model would have a negligible effect on the Coulomb cage volumes that we calculated with APBS. Thus, we argue that usage of an implicit solvent model is a reasonable approximation for the purpose of our analysis. Moreover, in a recent study, Cameron and co-workers performed MD simulations of Mhp1, a Na^{+}-hydantoin membrane transporter, by applying a full atomistic representation for the protein while the membrane was completely omitted [63]. However, we consider possible quantitative methodological ambiguities that can stem from the fact that an assignment of a uniform dielectric constant for a protein is physically meaningless; solvent-exposed surface, and residues that border water-bound vestibules should be described by different dielectric coefficients. Having said that, our results should be taken only as qualitative estimations and not as quantitative values.

Early models of *Vibrio parahaemolyticus* NhaA

Notably, two models for the *Vibrio parahaemolyticus* NhaA were generated by a fully automated protein structure homology modeling server [64]. These structures are part of a large repository database, and thus lack specific biochemical, biological and phylogenic considerations. As such, by removing the missing β-hairpin, they do not include residues 1 through 56 of the protein, leading to further absence of TMS I and connecting loops. Our model has integrated the phylogeny results and sequence homology to construct a model consisting all of the protein's residues. Additionally, our modeled protein was embedded in a membrane, and allowed to relax in a physiological environment. Thus, the final presented structure represents an MD-derived, whole and stable protein.

Concluding remarks

In this study, we have implemented phylogenetic analysis, homology modeling, evolutionary conservation data and MD simulation techniques aimed at suggesting a working model structure for the *Vibrio parahaemolyticus* NhaA. Using homology modeling, we constructed a preliminary model of the protein and evaluated its quality. Interestingly, based upon a phylogenetic analysis, we concluded that the preliminary model should lack the β-hairpin signature that the *Escherichia coli* possesses. The protein model was embedded in a lipid bilayer, rigorously energy minimized and subjected to an MD simulation. As a comparison, we simulated the *Escherichia coli* NhaA antiporter that was used as a template for our homology modeling process. We analyzed the overall three-dimensional structures of both proteins, followed their stability, calculated the essential

modes of motion and observed the characteristics of their internal vestibule and electrostatic potential. The model is supported not only by phylogenetic data, but by evolutionary data as well. The special characteristics of TMS X, previously reported by [16, 17], were noticeable and strengthened by our study as well. The majority of the model segments show evolutionary conservation whereas the variable residues are found mostly at the periphery and connecting loops. To our knowledge, the model represents the first example conformation of an antiporter that is β-hairpin-less and can also transport K^+.

Up to now, rational design of NhaA inhibitors has not been reported, and therefore having a blueprint structure of the *Vibrio parahaemolyticus* NhaA provides a basis for a functional analysis of the protein. Notably, *Vibrio parahaemolyticus* is the principle cause of seafood-associated bacterial gastroenteritis in the United States, and is responsible for food-borne outbreaks diseases at Asia [65], Africa [66] and South America [67]. Thus, the presented model in this study can be proved useful in virtual screening or de novo inhibitor design for discovery of new lead compounds. Considering that NHE1 (Na^+/H^+ exchanger 1) and NHA2 (Na^+/H^+ exchanger 2), the human orthologs to NhaA, bear no sequence similarity to NhaA, the latter may serve as a specific potent medical target for inhibition with relatively minor undesired side-effects to the host. Having said that, one should be aware that *Vibrio parahaemolyticus* contains several other reported Na^+ antiporters [15]. This raises doubts about the ability of specific inhibitors for NhaA to be potent drugs in fighting *Vibrio parahaemolyticus*. However, given that *Escherichia coli* contains more than one Na^+ antiporter (such as the NhaB or chaA porters) but only NhaA is crucial for Li^+ detoxification [9], it is not inconceivable that the *Vibrio parahaemolyticus* NhaA plays an essential role for the bacterial survival as well. We hope that our model will be considered useful from a mechanistic perspective and could be used in computational and structural dimerization studies of Na^+/H^+ proteins, ion selectivity, pH regulation or even for pharmaceutical purposes.

Acknowledgments This work was supported in part by grants from The Lady Davis Fellowship Trust and The Valazzi-Pikovsky Fellowship Fund (to A.G.), The Rudin Fellowship Trust (to R.A.) and the Israeli Science Foundation (784/01, 1249/05, 1581/08 to I.T.A.). I.T.A. is the Arthur Lejwa Professor of Structural Biochemistry at the Hebrew University of Jerusalem. The authors would like to thank Professor Aharon Oren from the Hebrew University of Jerusalem for fruitful discussions regarding bacterial phylogenetics.

References

1. West IC, Mitchell P (1974) Proton/sodium ion antiport in *Escherichia coli*. Biochem J 144(1):87–90
2. Orlowski J, Grinstein S (2004) Diversity of the mammalian sodium/proton exchanger SLC9 gene family. Pflugers Arch 447 (5):549–565
3. Padan E, Venturi M, Gerchman Y, Dover N (2001) Na^+/H^+ antiporters. Biochim Biophys Acta 1505(1):144–157
4. Goldberg EB, Arbel T, Chen J, Karpel R, Mackie GA, Schuldiner S, Padan E (1987) Characterization of a Na^+/H^+ antiporter gene of *Escherichia coli*. Proc Natl Acad Sci U S A 84 (9):2615–2619
5. Kuroda T, Shimamoto T, Inaba K, Tsuda M, Tsuchiya T (1994) Properties and sequence of the NhaA Na^+/H^+ antiporter of *Vibrio parahaemolyticus*. J Biochem 116(5):1030–1038
6. Ivey DM, Guffanti AA, Bossewitch JS, Padan E, Krulwich TA (1991) Molecular cloning and sequencing of a gene from alkaliphilic *Bacillus firmus* OF4 that functionally complements an *Escherichia coli* strain carrying a deletion in the NhaA Na^+/H^+ antiporter gene. J Biol Chem 266(34):23483–23489
7. Waser M, Hess-Bienz D, Davies K, Solioz M (1992) Cloning and disruption of a putative NaH-antiporter gene of *Enterococcus hirae*. J Biol Chem 267(8):5396–5400
8. Pinner E, Padan E, Schuldiner S (1992) Cloning, sequencing, and expression of the NhaB gene, encoding a Na^+/H^+ antiporter in *Escherichia coli*. J Biol Chem 267(16):11064–11068
9. Padan E (2008) The enlightening encounter between structure and function in the NhaA Na^+ /H^+ antiporter. Trends Biochem Sci 33 (9):435–443
10. Hunte C, Screpanti E, Venturi M, Rimon A, Padan E, Michel H (2005) Structure of a Na^+/H^+ antiporter and insights into mechanism of action and regulation by pH. Nature 435 (7046):1197–1202
11. Taglicht D, Padan E, Schuldiner S (1991) Overproduction and purification of a functional Na^+/H^+ antiporter coded by NhaA (ant) from *Escherichia coli*. J Biol Chem 266(17):11289–11294
12. Lacroix J, Pöet M, Maehrel C, Counillon L (2004) A mechanism for the activation of the Na/H exchanger NHE-1 by cytoplasmic acidification and mitogens. EMBO Rep 5(1):91–96
13. Padan E, Bibi E, Ito M, Krulwich TA (2005) Alkaline pH homeostasis in bacteria: new insights. Biochim Biophys Acta 1717(2):67–88
14. Olkhova E, Kozachkov L, Padan E, Michel H (2009) Combined computational and biochemical study reveals the importance of electrostatic interactions between the ”pH sensor” and the cation binding site of the sodium/proton antiporter NhaA of Escherichia coli. Proteins 76(3):548–559
15. Radchenko MV, Waditee R, Oshimi S, Fukuhara M, Takabe T, Nakamura T (2006) Cloning, functional expression and primary characterization of *Vibrio parahaemolyticus* K^+/H^+antiporter genes in Escherichia coli. Mol Microbiol 59(2):651–663
16. Kozachkov L, Herz K, Padan E (2007) Functional and structural interactions of the transmembrane domain X of NhaA, Na^+/H^+ antiporter of *Escherichia coli*, at physiological pH. Biochemistry 46(9):2419–2430
17. Olkhova E, Padan E, Michel H (2007) The influence of protonation states on the dynamics of the NhaA antiporter from *Escherichia coli*. Biophys J 92(11):3784–3791
18. Herz K, Rimon A, Jeschke G, Padan E (2009) Beta-sheet-dependent dimerization is essential for the stability of NhaA Na^+/H^+ antiporter. J Biol Chem 284(10):6337–6347
19. Gerchman Y, Rimon A, Venturi M, Padan E (2001) Oligomerization of NhaA, the Na^+/H^+ antiporter of *Escherichia coli* in the membrane and its functional and structural consequences. Biochemistry 40 (11):3403–3412
20. Hilger D, Jung H, Padan E, Wegener C, Vogel KP, Steinhoff HJ, Jeschke G (2005) Assessing oligomerization of membrane proteins by four-pulse DEER: pH-dependent dimerization of NhaA Na^+/H^+ antiporter of *E. coli*. Biophys J 89(2):1328–1338

21. Williams KA, Geldmacher-Kaufer U, Padan E, Schuldiner S, Kühlbrandt W (1999) Projection structure of NhaA, a secondary transporter from *Escherichia coli*, at 4.0 Å resolution. EMBO J 18 (13):3558–3563
22. Hilger D, Polyhach Y, Padan E, Jung H, Jeschke G (2007) High-resolution structure of a Na^+/H^+ antiporter dimer obtained by pulsed electron paramagnetic resonance distance measurements. Biophys J 93(10):3675–3683
23. Inoue H, Noumi T, Tsuchiya T, Kanazawa H (1995) Essential aspartic acid residues, Asp-133, Asp-163 and Asp-164, in the transmembrane helices of a Na^+/H^+ antiporter (NhaA) from *Escherichia coli*. FEBS Lett 363(3):264–268
24. Arkin IT, Xu H, Jensen MØ, Arbely E, Bennett ER, Bowers KJ, Chow E, Dror RO, Eastwood MP, Flitman-Tene R, Gregersen BA, Klepeis JL, Kolossvary I, Shan Y, Shaw DE (2007) Mechanism of Na^+/H^+ antiporting. Science 317(5839):799–803
25. Kelly MT, Stroh EM (1988) Temporal relationship of *Vibrio parahaemolyticus* in patients and the environment. J Clin Microbiol 26(9):1754–1756
26. McCarter L (1999) The multiple identities of *Vibrio parahaemolyticus*. J Mol Microbiol Biotechnol 1(1):51–57
27. Su YC, Liu C (2007) *Vibrio parahaemolyticus*: a concern of seafood safety. Food Microbiol 24(6):549–558
28. Torres J, Arkin IT (2000) Recursive use of evolutionary conservation data in molecular modeling of membrane proteins a model of the multidrug H^+ antiporter emrE. Eur J Biochem 267 (12):3422–3431
29. Ivetac A, Sansom MSP (2008) Molecular dynamics simulations and membrane protein structure quality. Eur Biophys J 37(4):403–409
30. Finn RD, Mistry J, Tate J, Coggill P, Heger A, Pollington JE, Gavin OL, Gunasekaran P, Ceric G, Forslund K, Holm L, Sonnhammer ELL, Eddy SR, Bateman A (2010) The Pfam protein families database. Nucleic Acids Res 38(Database issue): D211–222
31. Brenner DJ, Krieg NR, Staley JR, Garrity G (eds.) (2001) The Bergey's Manual of Systematic Bacteriology, vol. 2, 2nd edn. Springer
32. Maddison WP, Maddison DR. Mesquite: a modular system for evolutionary analysis. version 2.72. URL http://mesquiteproject.org/mesquite/mesquite.html
33. Altschul SF, Gish W, Miller W, Myers EW, Lipman DJ (1990) Basic local alignment search tool. J Mol Biol 215(3):403–410
34. Altschul SF, Madden TL, Schaffer AA, Zhang J, Zhang Z, Miller W, Lipman DJ (1997) Gapped BLAST and psi-BLAST: a new generation of protein database search programs. Nucleic Acids Res 25(17):3389–3402
35. Sali A, Blundell TL (1993) Comparative protein modelling by satisfaction of spatial restraints. J Mol Biol 234(3):779–815
36. Morris AL, MacArthur MW, Hutchinson EG, Thornton JM (1992) Stereochemical quality of protein structure coordinates. Proteins 12(4):345–364
37. Laskowski R, Macarthur M, Moss D, Thornton J (1993) PROCHECK: a program to check the stereochemical quality of protein structures. Journal of Applied Crystallography 26:283–291
38. Sippl MJ (1993) Recognition of errors in three-dimensional structures of proteins. Proteins 17(4):355–362
39. Wiederstein M, Sippl MJ (2007) ProSA-web: interactive web service for the recognition of errors in three-dimensional structures of proteins. Nucleic Acids Res 35:W407–W410
40. Lüthy R, Bowie JU, Eisenberg D (1992) Assessment of protein models with three-dimensional profiles. Nature 356(6364):83–85
41. Henikoff S, Henikoff JG (1992) Amino acid substitution matrices from protein blocks. Proc Natl Acad Sci U S A 89(22):10915–10919
42. Tieleman DP, Berendsen HJ (1998) A molecular dynamics study of the pores formed by *Escherichia coli* OmpF porin in a fully hydrated palmitoyloleoylphosphatidylcholine bilayer. Biophys J 74(6):2786–2801
43. Berendsen H, Postma J, van Gunsteren W, Hermans J, Pullman B (1981) Intermolecular forces: interaction models for water in relation to protein hydration. Reidel, Dordrecht
44. Van Der Spoel D, Lindahl E, Hess B, Groenhof G, Mark AE, Berendsen HJC (2005) GROMACS: fast, flexible, and free. J Comput Chem 26(16):1701–1718
45. Berendsen H, van der Spoel D, van Drunen R (1995) GROMACS - a message - passing parallel molecular dynamics implementation. Computer Physics Communications 91(1–3):43–56
46. Siu SWI, Vacha R, Jungwirth P, Bockmann RA (2008) Biomolecular simulations of membranes: physical properties from different force fields. J Chem Phys 128(12):125103
47. Hess B, Bekker H, Berendsen H, Fraaije J (1997) LINCS: a linear constraint solver for molecular simulations. J Comput Chem 18 (12):1463–1472
48. Darden T, York D, Pedersen L (1993) Particle mesh Ewald: an N-log(N) method for Ewald sums in large systems. Journal of Chemical Physics 98(12):10089–10092
49. Amadei A, Linssen AB, Berendsen HJ (1993) Essential dynamics of proteins. Proteins 17(4):412–425
50. Kleywegt GJ, Jones TA (1994) Detection, delineation, measurement and display of cavities in macromolecular structures. Acta Crystallogr D Biol Crystallogr 50(Pt 2):178–185
51. Rossmann MG, Arnold E (eds.) (2001) International tables for crystallography, Vol. F. Crystallography of Biological Macromolecules, chap. Around O, pp. 353–356, 366–367. Kluwer, Dordrecht
52. Baker NA, Sept D, Joseph S, Holst MJ, McCammon JA (2001) Electrostatics of nanosystems: application to microtubules and the ribosome. Proc Natl Acad Sci U S A 98(18):10037–10041
53. Olkhova E, Hunte C, Screpanti E, Padan E, Michel H (2006) Multiconformation continuum electrostatics analysis of the NhaA Na^+/H^+ antiporter of *Escherichia coli* with functional implications. Proc Natl Acad Sci U S A 103(8):2629–2634
54. Humphrey W, Dalke A, Schulten K (1996) VMD: visual molecular dynamics. J Mol Graph 14(1):33–38
55. Rimon A, Tzubery T, Padan E (2007) Monomers of the NhaA Na^+/H^+ antiporter of *Escherichia coli* are fully functional yet dimers are beneficial under extreme stress conditions at alkaline pH in the presence of Na^+ or Li^+. J Biol Chem 282(37):26810–26821
56. Forrest LR, Tang CL, Honig B (2006) On the accuracy of homology modeling and sequence alignment methods applied to membrane proteins. Biophys J 91(2):508–517
57. Donnelly D, Overington JP, Ruffle SV, Nugent JH, Blundell TL (1993) Modeling alpha-helical transmembrane domains: the calculation and use of substitution tables for lipid-facing residues. Protein Sci 2(1):55–70
58. Stevens TJ, Arkin IT (2001) Substitution rates in alpha-helical transmembrane proteins. Protein Sci 10(12):2507–2517
59. Torres J, Briggs JAG, Arkin IT (2002) Convergence of experimental, computational and evolutionary approaches predicts the presence of a tetrameric form for CD3-zeta. J Mol Biol 316 (2):375–384
60. Capener CE, Shrivastava IH, Ranatunga KM, Forrest LR, Smith GR, Sansom MS (2000) Homology modeling and molecular dynamics simulation studies of an inward rectifier potassium channel. Biophys J 78(6):2929–2942
61. Herz K, Rimon A, Olkhova E, Kozachkov L, Padan E (2010) Transmembrane segment II of NhaA Na^+/H^+ antiporter lines the cation passage, and Asp65 is critical for pH activation of the antiporter. J Biol Chem 285(3):2211–2220
62. Gv H (1986) The distribution of positively charged residues in bacterial inner membrane proteins correlates with the trans-membrane topology. EMBO J 5(11):3021–3027

63. Shimamura T, Weyand S, Beckstein O, Rutherford NG, Hadden JM, Sharples D, Sansom MSP, Iwata S, Henderson PJF, Cameron AD (2010) Molecular basis of alternating access membrane transport by the sodium-hydantoin transporter Mhp1. Science 328(5977):470–473
64. Kiefer F, Arnold K, Künzli M, Bordoli L, Schwede T (2009) The SWISS-MODEL repository and associated resources. Nucleic Acids Res 37(Database issue):D387–392
65. Pan TM, Chiou CS, Hsu SY, Huang HC, Wang TK, Chiu SI, Yea HL, Lee CL (1996) Food-borne disease outbreaks in Taiwan, 1994. J Formos Med Assoc 95(5):417–420
66. Ansaruzzaman M, Chowdhury A, Bhuiyan NA, Sultana M, Safa A, Lucas M, von Seidlein L, Barreto A, Chaignat CL, Sack DA, Clemens JD, Nair GB, Choi SY, Jeon YS, Lee JH, Lee HR, Chun J, Kim DW (2008) Characteristics of a pandemic clone of O3:K6 and O4: K68 *Vibrio parahaemolyticus* isolated in Beira, Mozambique. J Med Microbiol 57(Pt 12):1502–1507
67. Harth E, Matsuda L, Hernandez C, Rioseco ML, Romero J, Gonzalez-Escalona N, Martínez-Urtaza J, Espejo RT (2009) Epidemiology of *Vibrio parahaemolyticus* outbreaks, southern Chile. Emerg Infect Dis 15(2):163–168